On-Board Array Self-Calibration Using Amplitude-Only Proximal-Field Sensors and Machine-Learning-Based Phase Retrieval

Ailec Wu, Imaad A. Syed, Alex Ayling, Ali Hajimiri
Department of Electrical Engineering, California Institute of Technology, USA

***Abstract*— A technique for calibrating phased arrays using on-board proximal-field amplitude sensors is introduced. Using these sensors, the phase excitation of each element in an array is estimated using local measurements. This allows the array to self-calibrate and correct itself in the field with zero downtime. The sensors are implemented as low-complexity peak detectors, coupling a small amount of energy from the radiating elements and minimally affecting their performance. An information-theory-based sensor placement methodology is introduced. The resulting non-linear phase retrieval problem is solved using a convolutional neural network to predict the element phases. A proof-of-concept 2x4 array operating at 2.5GHz with proximal-field sensors is built and tested. The system achieves an average RMS phase error of 5.3 degrees.**

***Keywords*— self-calibration, inverse problems, microwave circuits, neural networks, phased arrays, supervised learning, phase retrieval**

I. Introduction

Phased arrays at microwave and millimeter wave frequencies provide high angular resolution, efficient spatial power combining, and dynamic electronic steering that benefit diverse applications such as communications, radar and wireless power transfer. A critical challenge in phased arrays is maintaining the timing/phase accuracy across all the elements in the array, particularly for large arrays. Calibration is required to bring the array to a known phase state and maintain the phase state under all operating conditions. This becomes increasingly challenging due to element phases drift over time and temperature, requiring additional calibration data to compensate. Real-time calibration allows the system to correct for this drift in highly dynamic environments.

Prior calibration techniques can be categorized as on-board or off-board [1]. Off-board calibration is typically performed in an anechoic chamber with a near- or far-field probe [2]. The phase of each element is measured and recorded in a look-up table prior to its deployment. The downside of this approach is that invariably the accuracy of the calibration will degrade as the system's operating environment changes or it ages, necessitating costly recalibration and potential downtime.

On-board calibration [3], [4], [5], [6], [7] requires no anechoic chamber, and can be done routinely in the field using hardware local to the array. One such procedure is to use the mutual coupling among the transmit and receive elements in the array to align the element phases [4], [5]. However, a limiting factor of this method is that the array must have co-located transmit and coherent receive elements, which is not always the case. Additionally, the array must be brought out of normal operation to run the calibration routine, which may be undesirable in applications like communications or wireless power transfer where the array needs to continuously deliver power to its receiver.

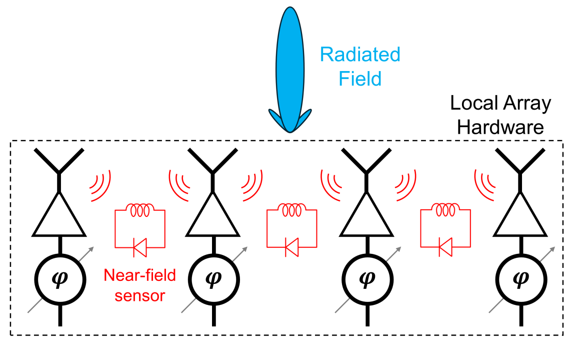

Fig. 1. Proximal-field amplitude sensors in a phased array.

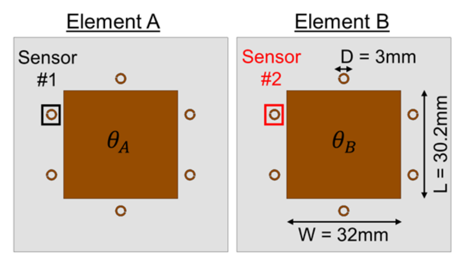

Fig. 2. Two-element array with patch antenna elements.

In this work, we use proximal-field sensors [3] to probe the near-field of the array while operating and use the sensors' outputs to determine the phase of all elements in the array (Fig. 1), allowing calibration to be done with no downtime. Furthermore, the sensors can be implemented as low-complexity peak detectors that measure only power. Amplitude-based sensors greatly simplify the electronics design and lower the cost, requiring only a diode detector circuit and no LO signal distribution. Additionally, the output is a low-frequency analog voltage that can be read and processed by a small A/D on a low-cost microcontroller. We also introduce an information-theoretic methodology to optimize sensor placement. To reconstruct the phase from the sensor measurements, a convolutional neural network is used to solve the resulting nonlinear inverse problem. This work demonstrates an on-board self-calibration system using amplitude-only measurements with zero downtime enabled by machine-learning-based phase retrieval.

II. Proximal Field Sensors

Described in detail in [3], proximal field sensors placed in close proximity of the radiators provide information about surrounding radiators by measuring small amounts of coupled power: it demonstrates relative phase prediction for a two-element phased array via proximal-field sensors capturing both amplitude and phase information.

Consider the sensors of the two-element array in Fig. 2 as the relative phase of the elements varies to gain intuition about their operation. Each sensor produces a sinusoidal interference pattern that has some amplitude and phase offset, which are functions of its position on the array. As the array size increases, coupling behavior between antennas and sensors becomes more complex due to the interference of multiple antennas at a given sensor. For sensors that yield both amplitude and phase, an array with n antenna drive ports and m receiving sensor ports can be viewed as an $(n+m)$-port black box. Given the system's $m \times n$ coupling sub-matrix between sensors (output) and transmit antennas (input), referred to as A, finding element phases from complex-valued sensors is straightforward matrix algebra:

$$\vec{\phi} = A^{-1}\begin{bmatrix}V_1 & V_2 & \cdots & V_n\end{bmatrix}^T = A^{-1}\vec{V}, \qquad (1)$$

where $\vec{V}$ is a vector of the received wave phasors read at the sensor ports, A is the coupling sub-matrix and $\vec{\phi}$ consists of the drive phasors. Taking the phase of each element of $\vec{\phi}$ gives the drive phases.

A might be inferred from simulation, or can be done by matrix inversion with a group of known element phase settings $\Phi = \begin{bmatrix}\phi_1 & \cdots & \phi_n\end{bmatrix}$ and corresponding sensor readings: $A = \vec{V}\Phi^{-1}$. In this approach, while coupling parameters might be inferred from simulation, coherent sensors requiring distribution of an RF signal incur high cost. Sensors providing only amplitude information (e.g., peak-detectors) avoid this complexity. However, amplitude-only sensors pose a new challenge, as finding the element phases is now a phase retrieval problem (often simple to state yet difficult to solve) [8], [9]:

$$\text{find } \vec{\phi}\text{, given } \begin{bmatrix}|A^1\vec{\phi}| & \cdots & |A^n\vec{\phi}|\end{bmatrix}^T, \qquad (2)$$

where A^k are the rows of the sub-matrix A. Finding A with amplitude-only sensors can also be shown to be a phase retrieval problem by following the technique outlined in [10].

A recent result indicates that, when n transmit antennas are present in the phased array (given the coupling sub-matrix is "generic"), $4n-4$ measurements are sufficient to recover phase information [11]. Thus, large arrays should have at least four amplitude-only sensors per antenna element.

III. Neural Networks

In this work, we propose usage of convolutional neural networks to directly infer element drive phases from amplitude-based sensor values. As mentioned in section II, amplitude-only proximal-field sensors require determination of both the coupling matrix and the inverse relationship between sensor readings and the corresponding antenna phases; the proposed neural network method can solve these nested phase-retrieval problems.

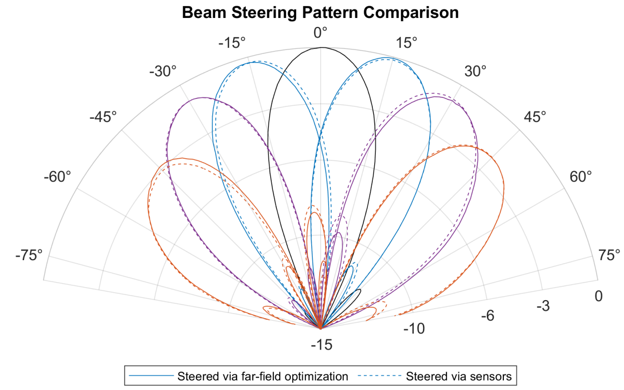

Fig. 3. Array far-field steering pattern measurements using far-field optimization (solid) and phase sensor feedback (dotted).

Usage of neural networks in phase retrieval applications is well-documented [12]; indeed, the problem of phase retrieval can be re-cast in a machine learning context as learning the weights of a single layer neural network with quadratic activation functions [8]. For usage here in the context of amplitude-only proximal-field sensors, the neural network method offers distinct advantages. Foremost, the method is flexible to different sensor and radiator setups. Furthermore, the method is convenient because it simultaneously handles both phase retrieval problems: determination of the coupling matrix and recovery of the antenna phases from sensor values. While the coupling pathways between antennas and sensors may be complex due to effects from surface waves, near-field radiation, and element interaction, sensor readings containing sufficient information should enable an effective model. Also, using neural networks on real hardware avoids discrepancies due to inaccurate simulation geometry and simulation error itself.

The proposed convolutional neural net model and training scheme are starting points and their refinement is ongoing. A limited Bayesian hyperparameter optimization was done for the network which, depicted in Fig. 4, features four convolutional layers followed by three fully connected layers (all layers are separated by ReLU activation [13]). To address the periodic nature of phase estimation in the loss function, output phases were encoded as in-phase and quadrature pairs. It was found that making the neural network predict the phase of each element relative to its top and left neighbor (a total of 20 output values) had better convergence; this output is later transformed into phases referenced to a single element. Training was done with the Adam algorithm [14].

IV. RF Design and Sensor Placement

A 2.5GHz probe-fed patch antenna is used as the unit element of the array. The antenna is fabricated on a 1.524mm (60mil) RO4350B substrate with length and width dimensions

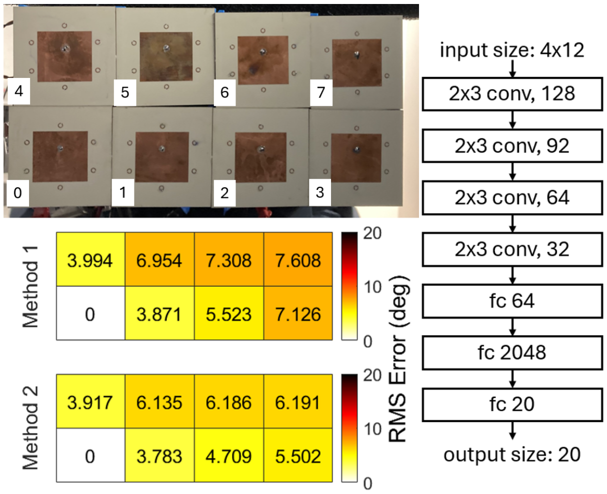

Fig. 4. 2x4 array element labeling (top left), RMS phase error heatmap for both methods (bottom left), and neural network block diagram (right)

shown in Fig. 2. Included in each antenna element are six loop sensors for probing the near-field. These loops are spread out around the antenna to sample the near-field at different locations. Each loop diameter is 3mm and is connected to an LTC5535 Schottky diode-based peak detector IC located on the backside of the PCB. The output of the sensor is an analog voltage that is low-pass filtered with a cutoff frequency of approximately 200kHz. The analog voltage is read by an ADC located on a low-cost ESP32 microcontroller. By spacing the loops appropriately from the antennas, their coupling coefficients range from -20dB to -23dB. This results in small a decrease of the antenna's radiation efficiency from 81.6% to 80.6%. Each antenna element is driven by a commercial power amplifier IC with a digitally programmable 8-bit phase shifter and 7-bit attenuator for phase and amplitude control. The power radiated by each element is approximately 20dBm.

While in this work sensor placement was done heuristically (with separate, identical antenna/sensor elements for rapid prototyping), we have developed an analytic method for systematic amplitude-only sensor placement. Intuitively, the optimal sensor placement provides the most unique information. Following information theory, we measure information as differential entropy [15], described as

$$H(I) = -\int_{-\infty}^{\infty} f_I(i)\log(f_I(i))di, \tag{3}$$

where $I(x, y)$ is the sensor power amplitude and $f_I(i)$ is the usual probability density function of $I(x, y)$. To generate these probability densities, we assume that all phases are uniform random variables ranging from 0 to 2π. It is also useful to measure redundancy with mutual information [15], defined as

$$M(I_1, I_2) = \int_{-\infty}^{\infty}\int_{-\infty}^{\infty} f_{I_1,I_2}(i_1, i_2)\log\left(\frac{f_{I_1,I_2}(i_1, i_2)}{f_{I_1}(i_1)f_{I_2}(i_2)}\right)di_1 di_2, \tag{4}$$

where $f_{I_1,I_2}(i_1, i_2)$ is the joint probability density function of the intensities. Taking inspiration from the "OBO"

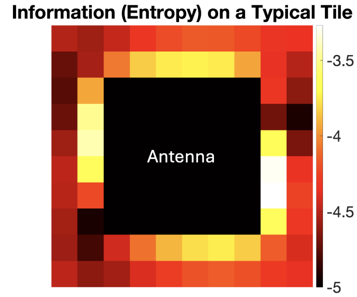

Fig. 5. Entropy values at various locations on a typical phased array tile. The antenna region has been blacked out.

approximation of mutual information in [16], we approximate conditional entropy as

$$H(i_1|(i_2, ..., i_n)) \approx H(i_1) - \sum_{k=2}^{n} M(i_1, i_k), \tag{5}$$

which is computed for a group of sensors indexed $1, .., n$. This allows for fast computation of conditional entropy at the cost of slight underestimation.

Sensor values are computed from coupling parameters by sweeping a set of sensors across tiles. With one sensor per tile, eight total sensors are swept to obtain the coupling parameters. The conditional entropy is calculated at all valid points on a tile and averaged over the eight tiles to generate a placement that can be tiled. As a visual for high information areas on such a phased array tile, an entropy map is provided in Fig. 5. Our initial algorithm maximized the objective function

$$\underset{S_l}{\operatorname{argmax}} \sum_{k=1}^{k=6} H(i_k|(S_l \setminus i_k)), \tag{6}$$

where $S_l = \{i_1, ..., i_6\}$ is the list of sensor location indices.

A placement is evaluated by first obtaining its corresponding A in simulation, followed by training a neural network on random phases for that placement; its RMS phase error denotes the quality of the placement. Simulations indicate that good placements require high unique information and high power. Restricting the placement region to a ring around the transmitting antenna and selecting the highest unique information set of equally spaced sensors has provided the best result so far: 2.97° RMS. Only using unique information results in 4.35° RMS, while only using high power locations results in 6.24° RMS.

V. Measurement

As a proof-of-concept, a 2x4 phased array using the unit cell described in section IV was assembled and placed on a far-field range. The array requires only a single far-field measurement to calibrate the phases to a known state, in this instance optimized to broadside [17]. Next, the training data was generated by uniformly sampling the phase shifter settings on each tile and recording corresponding sensor outputs. Done over a UART serial link, this takes approximately 30 minutes to generate a 100,000 point dataset of all 48 sensors. Element

0 (Fig. 4) is used as a reference element for the array, and its phase shifter is fixed to zero. Using the sensor readouts and labeled phase data, the neural network was then trained to predict each element's phase difference relative to its top and left neighbors. The training takes 50 minutes on a single Nvidia RTX 4090 GPU.

In order to determine phases referenced to element 0 from the neural network's prediction (phases relative to top and left neighbors), two methods are proposed. The first method uses either the top or the left prediction of each element to construct a tree; starting from the reference element, each element's phase is then calculated by propagation along the tree. The second method uses all of the neural network's relative phase predictions by formulating an overdetermined system of equations and calculating its pseudo-inverse while accounting for phase wrapping. The neural network's performance was verified by characterizing the phase error on an unbiased set of test data. This is shown in the heat maps of Fig. 4, displaying the RMS phase error at each element in the array.

For the more accurate method 2, the minimum phase error is 3.783° RMS at element 4 and maximum 6.191° RMS at element 7. The total phase error across all elements is approximately 5.3° RMS. The neural network's phase error takes an approximately normal distribution. As derived in [18], an infinite array with elements having uncorrelated Gaussian random variable phase errors of $<18^\circ$ RMS corresponds to less than 10% degradation in the beam efficiency of the array.

To verify the beam-steering capabilities of the neural network, the phase at each element was tuned to a desired phase gradient corresponding to $\pm 15^\circ$, $\pm 30^\circ$, and $\pm 45^\circ$ steering angles. Steering was accomplished using the sensor readouts and the corresponding neural network inferences to tune the phase setting with respect to the broadside state. Those results, compared with an optimized beam using the far-field range, are shown in Fig. 3. The neural network provides beam-steering angles very close to the desired value, with the phase error generally resulting in slight degradation of the side-lobe level.

VI. Conclusion

A self-calibrating system for phased arrays using proximal-field amplitude sensors was presented. This technique simplifies the electronics design by using power detectors as sensors, eliminating the need for high-frequency routing and minimizing the number of RF circuits. The phase is computed from these sensor values using a convolutional neural network, allowing the array to calibrate while operational.

Exciting future work in practical applications of this technique involves testing with larger arrays and including antenna amplitude information in the training data for power calibration. Theoretical work exploring more sophisticated methods of phase retrieval, training and refining the neural network, and sensor placement optimization should result in significant improvements in system performance.

Acknowledgment

The authors acknowledge the Caltech Space Solar Power Project for funding and support. We also thank Debjit Sarkar and Jatin Mathur for helpful comments and discussion.

References

[1] Z. Shafiq, D. E. Anagnostou, and S. K. Podilchak, "A computer controlled phase and magnitude self-calibration methodology for phased array antennas," *IEEE Journal of Microwaves*, vol. 4, no. 2, pp. 213–232, 2024.

[2] I. Şeker, "Calibration methods for phased array radars," in *Radar Sensor Technology XVII*, vol. 8714. SPIE, 2013, pp. 294–308.

[3] A. Safaripour, B. Asghari, M. R. M. Hashemi, and A. Hajimiri, "Proximal-field sensing: In situ prediction of far-field radiation for integrated radiators," *IEEE Transactions on Microwave Theory and Techniques*, vol. 67, no. 9, pp. 3743–3756, 2019.

[4] H. Aumann, A. Fenn, and F. Willwerth, "Phased array antenna calibration and pattern prediction using mutual coupling measurements," *IEEE Transactions on Antennas and Propagation*, vol. 37, no. 7, pp. 844–850, 1989.

[5] S. Shahramian, M. J. Holyoak, A. Singh, and Y. Baeyens, "A fully integrated 384-element, 16-tile, w -band phased array with self-alignment and self-test," *IEEE Journal of Solid-State Circuits*, vol. 54, no. 9, pp. 2419–2434, 2019.

[6] A. Nafe, K. Kibaroglu, M. Sayginer, and G. M. Rebeiz, "An in-situ self-test and self-calibration technique utilizing antenna mutual coupling for 5g multi-beam trx phased arrays," in *2019 IEEE MTT-S International Microwave Symposium (IMS)*, 2019, pp. 1229–1232.

[7] A. Fikes, O. S. Mizrahi, and A. Hajimiri, "A framework for array shape reconstruction through mutual coupling," *IEEE Transactions on Microwave Theory and Techniques*, vol. 69, no. 10, pp. 4422–4436, 2021.

[8] J. Dong, L. Valzania, A. Maillard, T.-a. Pham, S. Gigan, and M. Unser, "Phase retrieval: From computational imaging to machine learning: A tutorial," *IEEE Signal Processing Magazine*, vol. 40, no. 1, pp. 45–57, 2023.

[9] K. Jaganathan, Y. C. Eldar, and B. Hassibi, *Phase retrieval: an overview of recent developments*. CRC Press, Oct 2016, p. 263–296.

[10] D. Kogan, Y. C. Eldar, and D. Oron, "On the 2d phase retrieval problem," *IEEE Transactions on Signal Processing*, vol. 65, no. 4, pp. 1058–1067, 2017.

[11] A. Conca, D. Edidin, M. Hering, and C. Vinzant, "An algebraic characterization of injectivity in phase retrieval," *Applied and Computational Harmonic Analysis*, vol. 38, no. 2, p. 346–356, Mar. 2015. [Online]. Available: http://dx.doi.org/10.1016/j.acha.2014.06.005

[12] Y. Rivenson, Y. Zhang, H. Günaydın, D. Teng, and A. Ozcan, "Phase recovery and holographic image reconstruction using deep learning in neural networks," *Light: Science & Applications*, vol. 7, no. 2, pp. 17 141–17 141, Feb 2018.

[13] A. F. Agarap, "Deep learning using rectified linear units (relu)," 2019. [Online]. Available: https://arxiv.org/abs/1803.08375

[14] D. P. Kingma and J. Ba, "Adam: A method for stochastic optimization," 2017. [Online]. Available: https://arxiv.org/abs/1412.6980

[15] T. M. Cover and J. A. Thomas, *Chapter 8 - Differential Entropy, Elements of Information Theory, 2nd ed.* Hoboken, New Jersey: Wiley-Interscience, 2006.

[16] J. González-López, S. Ventura, and A. Cano, "Distributed selection of continuous features in multilabel classification using mutual information," *IEEE Transactions on Neural Networks and Learning Systems*, vol. 31, no. 7, pp. 2280–2293, 2020.

[17] A. Hajimiri, B. Abiri, F. Bohn, M. Gal-Katziri, and M. H. Manohara, "Dynamic focusing of large arrays for wireless power transfer and beyond," *IEEE Journal of Solid-State Circuits*, vol. 56, no. 7, pp. 2077–2101, 2021.

[18] J. A. Nanzer, R. L. Schmid, T. M. Comberiate, and J. E. Hodkin, "Open-loop coherent distributed arrays," *IEEE Transactions on Microwave Theory and Techniques*, vol. 65, no. 5, pp. 1662–1672, 2017.